Electron Rich Cluster Chemistry: Synthesis and Molecular and Electronic Structures of the Series of Clusters $Ru_4(CO)_{13}(\mu\text{-}PR_2)_2$ with Expanded Metal Frameworks

John F. Corrigan, Marie Dinardo, Simon Doherty, Graeme Hogarth, Yan Sun, Nicholas J. Taylor, and Arthur J. Carty*

Guelph-Waterloo Centre for Graduate Work in Chemistry, Waterloo Campus, Department of Chemistry, University of Waterloo, Waterloo, Ontario N2L 3G1, Canada

Received March 14, 1994[⊗]

The reaction of 2 equiv of dialkyl-, diaryl-, dialkoxy- or bis(dialkylamino)chlorophosphines, R_2PCl (R = Cy, Et, OEt, NPr^i_2, Ph, Pr^i), with the 60-electron tetrahedral cluster anion $[Ru_4(CO)_{13}]^{2-}$ results in the partial opening of the Ru_4 framework and the formation of $[Ru_4(CO)_{13}(\mu\text{-}PR_2)_2]$ (**1a**, R = Ph; **1b**, R = Pr^i; **1c**, R = OEt; **1d**, R = NPr^i_2; **1e**, R = Cy; **1f**, R = Et) in varying fields. These 64-electron phosphido-bridged clusters consist of planar Ru_4 butterfly polyhedra possessing two normal and three elongated metal–metal bonds. The compounds have been fully characterized by IR and ^1H, ^{31}P, and ^{13}C NMR spectroscopy. Single-crystal X-ray structure determinations of **1a**–**d** are also reported. Crystal data for **1a**: $Ru_4P_2O_{13}C_{37}H_{20}\cdot 2CHCl_3$, orthorhombic, space group $P2_12_12$, $a = 11.463(2)$ Å, $b = 15.818(3)$ Å, $c = 13.071(3)$ Å, $Z = 2$. The structure was solved and refined to $R = 0.0221$ and $R_w = 0.0223$ on the basis of 3411 observed ($F \geq 6.0\sigma(F)$) reflections. Crystal data for **1b**: $Ru_4P_2O_{13}C_{25}H_{28}\cdot CHCl_3$, triclinic, space group $P\bar{1}$, $a = 11.169(1)$ Å, $b = 12.488(2)$ Å, $c = 14.040(3)$ Å, $\alpha = 82.48(2)°$, $\beta = 80.94(1)°$, $\gamma = 84.46(1)°$, $Z = 2$. Refinement converged at $R = 0.0225$ and $R_w = 0.0263$ on the basis of 5765 observed data. Crystal data for **1c**: $Ru_4P_2O_{17}C_{21}H_{20}\cdot {}^1/_2C_6H_6$, triclinic, space group $P\bar{1}$, $a = 9.273(2)$ Å, $b = 11.269(2)$ Å, $c = 17.512(2)$ Å, $\alpha = 78.83(2)°$, $\beta = 81.89(2)°$, $\gamma = 77.23(2)°$, $Z = 2$. The final R and R_w values obtained were 0.0258 and 0.0322, respectively, using 7244 observed reflections. Crystal data for **1d**: $Ru_4P_2N_4O_{13}C_{37}H_{56}$, monoclinic, space group $P2_1/m$, $a = 9.889(1)$ Å, $b = 23.913(3)$ Å, $c = 10.789(1)$ Å, $\beta = 106.96(2)°$, $Z = 2$. The structure was solved and refined to $R = 0.0243$ and $R_w = 0.0259$ for 4388 observed data. The clusters **1a**–**d** exhibit significantly different elongation patterns of the Ru–Ru and Ru–P vectors as a consequence of the varying electronic effects of the phosphido bridges, a fact confirmed by EHMO calculations. All of the compounds **1a**–**f** have a ^{31}P NMR resonance which is more shielded than in phosphido bridges across normal ruthenium–ruthenium bonds.

Introduction

Polynuclear transition-metal clusters with electron counts and framework molecular geometries consistent with the predictions of the 18-electron rule or effective atomic number rules are described as electron precise. Within the regime of tetrametal clusters, for example, the numbers of cluster valence electrons, two-center–two-electron metal–metal bonds, and molecular shapes are shown in Chart 1. Electron-precise tetrahedral, butterfly, and rectangular or metal-coordinated triangular clusters have six, five, and four metal–metal bonds, respectively, and are associated with 60-, 62-, and 64-electron counts. It follows that molecules having these structural features yet possessing more or fewer electrons than the electron-precise count may be termed electron rich or electron deficient. Thus, a cluster with a butterfly structure and five metal–metal interactions is electron precise with 62 cluster valence electrons but *electron rich* with 64 electrons. There are many clusters which fall into the class of electron-deficient molecules, particularly for transition metals such as platinum or gold, where the full sets of s and p orbitals are not used

Chart 1

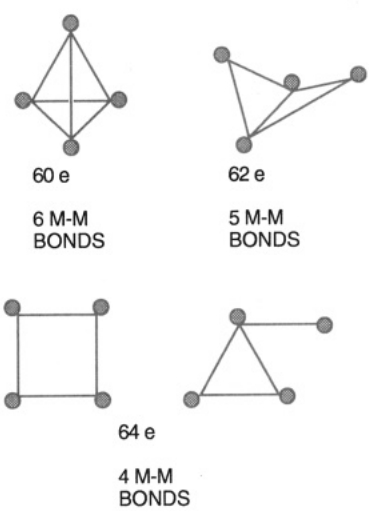

[⊗] Abstract published in *Advance ACS Abstracts,* July 15, 1994.

0276-7333/94/2313-3572$04.50/0

in cluster bonding.[1] In contrast, the class of electron-rich clusters has until recently received little attention and the relationship of molecular structure to cluster reactivity has not been thoroughly explored.[2] This paper highlights recent developments in electron rich cluster chemistry[3] and describes in detail the structural features of an extensive class of unusual 64-electron molecules **1** having rhomboidal (or flat butterfly) geometries.[4] With five Ru—Ru bonding contacts, these clusters are formally electron rich. We have shown that the $M_4(\mu\text{-}PR_2)_2$ framework of these electron-rich clusters $[Ru_4(CO)_{13}(\mu\text{-}PR_2)_2]$ is remarkably thermally resistant to fragmentation under forcing conditions and that these molecules are able to alleviate their electronic oversaturation via carbonyl loss.[4b,c] Addition and elimination reactions proceed in high yield, with retention of the tetranuclear metal framework, accompanied by skeletal rearrangement and intramolecular ligand activation. Cluster fragmentation/degradation has often been observed under the robust conditions required to initiate reactivity. Both of these potential difficulties are circumvented with **1a**–**f**.

The results of extended Hückel molecular orbital (EHMO) calculations on **1** and the correlation of electronic and molecular structures in these cluster systems are also described.

Experimental Section

General Procedures. Syntheses were carried out using either an inert-atmosphere MBraun glovebox or standard Schlenk-line techniques on a double-manifold vacuum line with high-purity, dry nitrogen. Solvents for reactions, chromatography, and crystallizations were distilled under nitrogen from appropriate drying agents prior to use. Separation of the products was accomplished by column chromatography using oven-dried (150 °C, 48 h) silica gel (70–230 mesh) on a dry-packed 3 × 20 cm column. All reactions were monitored by thin-layer chromatography (Baker Flex, silica gel 1B-F) and infrared spectroscopy (carbonyl region). Solution infrared spectra (NaCl, 0.5-mm matched cells) were recorded on a Nicolet 520 FTIR spectrometer. Proton NMR spectra were recorded on Bruker AC-200 and AM-250 instruments, and chemical shifts are referenced internally to the protio impurities of the deuterated solvents. $^{13}C\{^1H\}$ NMR spectra were similarly run at 50.32 and 62.97 MHz, respectively, and are referenced to the ^{13}C resonance of the solvent. Broad-band $^{31}P\{^1H\}$ NMR spectra were obtained on the same instruments operating at 81.02 and 101.27 MHz, respectively, externally referenced to $P(OMe)_3$. ^{31}P (solution) chemical shifts are reported relative to H_3PO_4. Microanalyses were performed by M-H-W Laboratories, Phoenix, AZ. Starting materials were obtained from the following suppliers: triruthenium dodecacarbonyl and diphenyl-, diethyl-, and dicyclohexylchlorophosphine from Strem, diethoxy-, diisopropyl-, and bis(diisopropylamino)chlorophosphine from Aldrich, potassium metal from J. T. Baker, and diphenyl ketone from BDH Laboratories. All chemicals were used as supplied. The potassium salt of the dianion $[Ru_4(CO)_{13}]^{2-}$ was prepared through a modification of the literature procedure.[5]

Synthesis of $[Ru_4(CO)_{13}(\mu\text{-}PPh_2)_2]$ (1a). To a Schlenk tube containing $[Ru_3(CO)_{12}]$ (0.49 g, 0.77 mmol), diphenyl ketone (0.21 g, 1.15 mmol), and potassium metal (0.045 g, 1.15 mmol) was added 20 mL of tetrahydrofuran, dropwise over a period of 20 min, with constant stirring. The suspension was stirred for 24–26 h until the reduction of $[Ru_3(CO)_{12}]$ was complete. To the resultant cherry red solution was added, dropwise, diphenylchlorophosphine (0.21 mL, 1.15 mmol), and the solution was stirred for an additional 2 h. The solvent was removed under reduced pressure and the residue extracted with CH_2Cl_2. The methylene chloride solution was absorbed onto silica and desolvated. Elution with dichloromethane/*n*-hexane (1/10 v/v) afforded a pale yellow band, identified as $[Ru_3(CO)_{12}]$, and a dark red band of **1a**, and the compound was recrystallized from a concentrated dichloromethane/*n*-hexane solution at −10 °C. Yield: 0.19 g (29%). Anal. Calcd for $Ru_4P_2O_{13}C_{37}H_{20}$ (**1a**): C, 39.03; H, 1.77. Found: C, 39.09; H, 1.90. IR (C_6H_{12}): ν(CO) 2077 m, 2043 s, 2039 m, 2032 w, 2010 m, 1991 m cm^{-1}. $^{31}P\{^1H\}$ NMR (C_6D_6): δ 118.8 (s) ppm. ^1H NMR (CD_2Cl_2): δ 7.98 (m, 8H, H_{ortho}), 7.41 (m, 12H, $H_{meta,para}$). $^{13}C\{^1H\}$ NMR (CD_2Cl_2): δ 207.5 (s, CO), 196.9 (s, CO), 196.5 (s, CO), 190.4 (t, J_{PC} = 10.8 Hz), 141.0 (virtual triplet, J_{PC} = 15.6 Hz, C_{ipso}), 133.2 (virtual triplet, J_{PC} = 6.2 Hz, C_{ortho}), 130.5 (s, C_{para}), 129.2 (virtual triplet, J_{PC} = 4.5 Hz, C_{meta}).

Synthesis of $[Ru_4(CO)_{13}(\mu\text{-}PPr^i_2)_2]$ (1b). Compound **1b** was prepared in a manner similar to that described above. Yield: 34%. Anal. Calcd for $Ru_4P_2O_{13}C_{25}H_{28}$ (**1b**): C, 29.95; H, 2.81. Found: C, 29.75; H, 3.00. IR (C_6H_{12}): ν(CO) 2063 m, 2027 m, 2022 s, 1997 w, 1992 m, 1986 w cm^{-1}. $^{31}P\{^1H\}$ NMR ($CDCl_3$): δ 149.4 (s) ppm. ^1H NMR ($CDCl_3$): δ 2.46 (septet, 4H, J_{HH} = 7.2 Hz, C—C*H*—C), 1.66 (dd, 24 H, J_{PH} = 14.7 Hz, J_{HH} = 7.2 Hz, H_3C—C). $^{13}C\{^1H\}$ NMR ($CDCl_3$): δ 209.4 (s, CO), 201.4 (br, CO), 196.6 (s, CO), 196.1 (s, CO), 192.0 (br, CO), 37.5 (virtual triplet, J_{PC} = 5.7 Hz, C—*C*H—C), 24.6 (d, J_{PC} = 51.9 Hz, H_3C—C).

Synthesis of $[Ru_4(CO)_{13}\{\mu\text{-}P(OEt)_2\}_2]$ (1c). The compound **1c** was prepared in a manner similar to that described for **1a**. Recrystallization was carried out in benzene/methanol (1/5 v/v) at −10 °C. Yield: 16%. Anal. Calcd for

(1) Mingos, D. M. P.; Wales, D. J. *Introduction to Cluster Chemistry*; Prentice-Hall: Englewood Cliffs, NJ, 1990; Chapter 4 and references therein.

(2) Mingos, D. M. P.; May, A. S. In *The Chemistry of Metal Cluster Complexes*; Shriver, D. F., Kaesz, H. D., Adams, R. D., Eds.; VCH: New York, 1990; Chapter 2.

(3) For examples of such expanded frameworks see the following. (i) Ru_3 clusters: (a) Lugan, N.; Fabre, P.-L.; de Montauzon, D.; Lavigne, G.; Bonnet, J.-J.; Saillard, J.-Y.; Halet, J. F. *Inorg. Chem.* **1993**, *32*, 1363. (b) Lugan, N.; Lavigne, G.; Bonnet, J. J.; Rean, R.; Neibecker, D.; Tkatchenko, I. *J. Am. Chem. Soc.* **1988**, *110*, 5369. (c) Cabeza, J. A.; Lahoz, F. J.; Martin, A. *Organometallics* **1992**, *11*, 2754. (d) Corrigan, J. F.; Doherty, S.; Taylor, N. J.; Carty, A. J.; Boroni, E.; Tiripicchio, A. *J. Organomet. Chem.* **1993**, *462*, C24. (ii) Os_3 clusters: (e) Cherkas, A. A.; Taylor, N. J.; Carty, A. J. *J. Chem. Soc., Chem. Commun.* **1990**, 385. (iii) Ru_4/Os_4 clusters: (f) Carty, A. J.; MacLaughlin, S. A.; Wagner, J. V.; Taylor, N. J. *Organometallics* **1982**, *1*, 1013. (g) Churchill, M. R.; Bueno, C.; Young, D. A. *J. Organomet. Chem.* **1981**, *213*, 139. (h) Mul, W. P.; Elsevier, C. J.; van Leijen, M.; Vrieze, K.; Smeets, W. J. J.; Spek, A. l. *Organometallics* **1992**, *11*, 1877. (i) Adams, R. D.; Yang, L. W. *J. Am. Chem. Soc.* **1983**, *105*, 235. (j) Hogarth, G.; Phillips, J. A.; van Gastel, F.; Taylor, N. J.; Marder, T. B.; Carty, A. J. *J. Chem. Soc., Chem. Commun.* **1988**, 1570. (iv) Pt_3 clusters: (k) Pergola, D. R.; Garlaschelli, L.; Mealli, C.; Proserpio, D. M.; Zanello, P. *J. Cluster Sci.* **1990**, *1*, 93. (l) Longoni, G.; Manassero, M.; Sansoni, S. *J. Am. Chem. Soc.* **1980**, *102*, 7973. (m) Taylor, N. J.; Chieh, P. C.; Carty, A. J. *J. Chem. Soc., Chem. Commun.* **1975**, 448. (n) Bender, R.; Braunstein, P.; Tiripicchio, A.; Tiripicchio-Camellini, M. *Angew. Chem., Int. Ed. Engl.* **1985**, *24*, 861. (v) Pd_3 clusters: (o) Bushnell, G. W.; Dixon, K. R.; Moroney, P. M.; Rattray, A. D.; Wan, C. *J. Chem. Soc., Chem. Commun.* **1977**, 709. (vi) Ru_5 clusters: (p) Adams, C. J.; Bruce, M. I.; Liddell, M. J.; Skelton, B. W.; White, A. H. *J. Chem. Soc., Chem. Commun.* **1992**, 1314. (q) Adams, C. J.; Bruce, M. I.; Skelton, B. W.; White, A. H. *J. Chem. Soc., Dalton Trans.* **1992**, 3057. (vii) Ni_5 clusters: (r) Longoni, G.; Chini, P.; Lower, L. D.; Dahl, L. F. *J. Am. Chem. Soc.* **1975**, *97*, 5034. (viii) Rh_3/Ir_3 clusters: (s) Berry, D. E.; Browning, J.; Dehghan, K.; Dixon, K. R.; Meanwell, N. J.; Phillips, A. J. *Inorg. Chem.* **1991**, *30*, 396. (t) Haines, R. J.; Steen, N. D. C. T., English, R. B. *J. Chem. Soc., Dalton Trans.* **1984**, 515.

(4) (a) Sappa, E.; Tiripicchio, A.; Toogood, G. E.; Carty, A. J. *Prog. Inorg. Chem.* **1987**, *35*, 407. (b) Corrigan, J. F.; Doherty, S.; Taylor, N. J.; Carty, A. J. *Organometallics* **1992**, *12*, 993. (c) Corrigan, J. F.; Doherty, S.; Taylor, N. J.; Carty, A. J. *J. Am. Chem. Soc.* **1992**, *114*, 7557. (d) Hogarth, G.; Hadj-Bagheri, N.; Taylor, N. J.; Carty, A. J. *J. Chem. Soc., Chem. Commun.* **1990**, 1352. (e) Corrigan, J. F.; Dinardo, M.; Doherty, S.; Carty, A. J. *J. Cluster Sci.* **1992**, *3*, 313. (f) Corrigan, J. F.; Sun, Y.; Carty, A. J. *New J. Chem.* **1994**, *18*, 77.

(5) Bhattacharyya, A. K.; Nagel, C. C.; Shore, S. G. *Organometallics* **1983**, *2*, 1187.

Table 1. Crystallographic Data for 1a–d

chem formula	$Ru_4P_2O_{13}C_{37}H_{20}{\cdot}2CHCl_3$	$Ru_4P_2O_{13}C_{25}H_{28}{\cdot}CHCl_3$	$Ru_4P_2O_{17}C_{21}H_{20}{\cdot}^1/_2C_6H_6$	$Ru_4P_2N_4O_{13}C_{37}H_{56}$
cryst syst	orthorhombic	triclinic	triclinic	monoclinic
space group	$P2_12_12$	$P\bar{1}$	$P\bar{1}$	$P2_1/m$
a, Å	11.463(2)	11.169(1)	9.273(2)	9.889(1)
b, Å	15.818(3)	12.488(2)	11.269(2)	23.913(3)
c, Å	13.071(3)	14.040(3)	17.512(2)	10.789(1)
α, deg		82.48(2)	73.83(2)	
β, deg		80.94(1)	81.89(2)	106.96(2)
γ, deg		84.46(1)	77.23(2)	
V, Å^3	2369.9(9)	1911.5(6)	1741.8(5)	2440.3(5)
Z	2	2	2	2
fw	1377.5	1122.1	1049.6	1231.1
T, K	200	200	200	200
λ, Å	0.710 73 (Mo Kα)	0.710 73 (Mo Kα)	0.710 73 (Mo Kα)	0.710 73 (Mo Kα)
ϱ_{calcd}, g cm^{-3}	1.930	1.950	2.001	1.675
μ, cm^{-1}	17.16	18.71	18.63	13.39
R^a	0.0221	0.0225	0.0258	0.0243
$R_w{}^b$	0.0223	0.0263	0.0322	0.0259

$^a R = \Sigma(|F_o| - |F_c|)/\Sigma|F_o|$. $^b R_w = [\Sigma w(|F_o| - |F_c|)^2/\Sigma w F_o^2]^{1/2}$.

$Ru_4P_2O_{13}C_{21}H_{20}{\cdot}0.5C_6H_6$ (**1c**): C, 27.46; H, 2.21. Found: C, 27.26; H, 2.34. IR (C_6H_{12}): ν(CO) 2077 m, 2044 s, 2028 w, 2010 m, 2000 w, 1992 m cm^{-1}. $^{31}P\{^1H\}$ NMR ($CDCl_3$): δ 302.3 (s) ppm. ^1H NMR ($CDCl_3$): δ 4.12 (mult, 8H, $-CH_2-$), 1.32 (t, 12H, J_{HH} = 7.0 Hz, $-CH_3$) ppm. $^{13}C\{^1H\}$ NMR ($CDCl_3$): δ 206.7 (t, J_{PC} = 5.0 Hz, CO), 202.0 (s, CO), 196.6 (s, CO), 195.7 (s, CO), 186.5 (t, J_{PC} = 12.5 Hz, CO), 67.2 (virtual triplet, J_{PC} = 3.5 Hz, $-CH_2-$), 16.2 (virtual triplet, J_{PC} = 4.0 Hz, $-CH_3$) ppm.

Synthesis of $[Ru_4(CO)_{13}\{\mu\text{-}P(NPr^i_2)_2\}_2]$ (1d). The compound was prepared as described above. Separation on silica gel (eluant *n*-hexane) and recrystallization from dichloromethane/methanol (1/5 v/v) afforded red-purple crystals of **1d**. Yield: 65%. Anal. Calcd for $Ru_4P_2O_{13}N_4C_{37}H_{56}$ (**1d**): C, 36.10; H, 4.59; N, 4.55. Found: C, 35.95; H, 4.71; N, 4.48. IR (C_6H_{12}): ν(CO) 2096 w, 2061 m, 2029 s, 2025 s, 1999 w, 1987 m, 1981 m, 1971 vw, 1963 vw cm^{-1}. $^{31}P\{^1H\}$ NMR ($CDCl_3$): δ 235.5 (s) ppm. ^1H NMR ($CDCl_3$): δ 4.38 (septet, 8H, J_{HH} = 6.4 Hz, $-CH(CH_3)_2$), 1.41 (t, 48H, J_{HH} = 6.4 Hz, $-CH(CH_3)_2$) ppm. $^{13}C\{^1H\}$ NMR ($CDCl_3$): δ 209.5 (s, CO), 201.8 (s, CO), 198.4 (s, CO), 197.0 (s, CO), 190.4 (t, J_{PC} = 10.6 Hz, CO), 53.9 (s, $-CH(CH_3)_2$), 24.7 (s, $-CH(CH_3)_2$) ppm.

Synthesis of $[Ru_4(CO)_{13}(\mu\text{-}PCy_2)_2]$ (1e). The preparation and purification of **1e** were carried out as for **1a**. Yield: 33%. Anal. Calcd for $Ru_4P_2O_{13}C_{37}H_{44}$ (**1e**): C, 38.21; H, 3.81. Found: C, 38.16; H, 3.89. IR (C_6H_{12}): ν(CO) 2061 m, 2025 m, 2019 s, 1995 w, 1990 w, 1985 w cm^{-1}. $^{31}P\{^1H\}$ NMR ($CDCl_3$): δ 143.6 (s) ppm. ^1H NMR ($CDCl_3$): δ 2.33–1.29 (br mult) ppm. $^{13}C\{^1H\}$ NMR ($CDCl_3$): δ 209.7 (s, CO), 201.6 (br, CO), 197.1 (s, CO), 196.3 (s, CO), 192.3 (br, CO), 48.6 (br s, $-CH_2-CH-CH_2-$), 35.7 (d, J_{PC} = 53.3 Hz, $-CH-CH_2-CH_2$), 28.3 (d, J_{PC} = 5.4 Hz, $-CH_2-CH_2-CH_2-$), 26.2 (s, $-CH_2$) ppm.

Synthesis of $[Ru_4(CO)_{13}(\mu\text{-}PEt_2)_2]$ (1f). The preparation and purification of **1f** were carried out as for **1a**. Yield: 19%. Anal. Calcd for $Ru_4P_2O_{13}C_{21}H_{20}$ (**1f**): C, 26.65; H, 2.13. Found: C, 26.80; H, 2.33. IR (C_6H_{12}): ν(CO) 2065 s, 2028 s, 2022 vs, 1998 w, 1993 m, 1988 w cm^{-1}. $^{31}P\{^1H\}$ NMR ($CDCl_3$): δ 111.3 (s) ppm. ^1H NMR ($CDCl_3$): δ 2.44 (qd, 8H, J_{PH} = 1.6 Hz, J_{HH} = 7.4 Hz, $-CH_2-$), 1.45 (dt, 12H, J_{PH} = 17.7 Hz, J_{HH} = 7.4 Hz, CH_3-) ppm. $^{13}C\{^1H\}$ NMR ($CDCl_3$): δ 208.8 (s, CO), 201.8 (br, CO), 195.9 (s, CO), 195.6 (s, CO), 190.9 (t, J_{PC} = 10.7 Hz, CO), 24.7 (virtual triplet, J_{PC} = 8.6 Hz, $-CH_2-$), 12.6 (s, CH_3-) ppm.

X-ray Structural Analyses of 1a–d. Dark red crystals of **1a** suitable for X-ray analysis were obtained from the slow evaporation of concentrated $CH_2Cl_2/CHCl_3$ solutions at 295 K. Crystals of **1b,d** were grown at −10 °C from $CHCl_3/C_7H_{16}$, and those of **1c** were obtained from a C_6H_6/CH_3OH mixture at −10 °C. Suitable crystals of each cluster were glued to glass fibers using epoxy resin, mounted on a goniometer head, and centered on an LT-2-equipped Siemens R3m/V diffractometer. Unit cell parameters were obtained for each crystal from the least-squares refinement of the setting angles of 25 reflections well dispersed ($20 \le 2\theta \le 30°$) in reciprocal space.

Collection and Reduction of the Intensity Data. Details of the intensity data collection are summarized in Table 1. Intensity data for **1a–d** were measured at 200 K using graphite-monochromated Mo Kα (λ = 0.710 73 Å) radiation and the ω-scan technique with a variable scan speed. Background measurements for all data were made at the beginning and end of each scan, each for 25% of the total scan time. Two standard reflections monitored every 100 reflections indicated no significant changes during the data collection.

Solution and Refinement of the Intensity Data. In all four cases, Patterson syntheses readily yielded the positions of the metal atoms and standard Fourier methods were used to locate the remaining non-hydrogen atoms. Full-matrix least-squares refinement of positional and thermal parameters were followed by subsequent conversion to anisotropic thermal coefficients for all non-hydrogen atoms. The hydrogen atom positions were located in the final difference Fourier maps and were included in calculated positions and refined isotropically. The function minimized in the least-squares refinement was $\Sigma w(|F_o| - |F_c|)^2$. The weighted R value, R_w, is defined as $[\Sigma w(|F_o| - |F_c|)^2/\Sigma w|F_o|^2]^{1/2}$, where the weights, w, are optimized on moderate intensities. Absorption corrections were applied using the face-indexed numerical method for all crystals. Atomic scattering factors used, including anomalous dispersion corrections for ruthenium, were taken from ref 6a, and those of Stewart *et al.*[6b] were used for the hydrogen atoms. All calculations were performed on a Microvax II and Vax 3000 using SHELXTL PLUS software. The absolute configuration of **1a** was determined using the collected Friedel opposites. Refinement of the structure using the unmerged data (5952 reflections) gave R and R_w values for the correct enantiomorph of 0.0271 and 0.0269, respectively. The opposite (incorrect) enantiomorph yielded R = 0.0291 and R_w = 0.0301.

Results and Discussion

The butterfly arrangement of metal atoms has attracted much attention due to the structural and electronic versatility often exhibited within this class of molecule.[4a,7] Following our initial communication describing the route to $[Ru_4(CO)_{13}(\mu\text{-}PPh_2)_2]$ (**1a**),[3j] we

(6) (a) *International Tables for X-ray Crystallography*; Kynoch Press: Birmingham, England, 1974; Vol. 4. (b) Stewart, R. F.; Davidson, E. R.; Simpson, W. T. *J. Chem. Phys.* **1965**, *42*, 3175.

(7) (a) Braunstein, P.; de Méric de Bellefon, C.; Bouaoud, S.-E.; Grandjean, D.; Halet, J.-F.; Saillard, J.-Y. *J. Am. Chem. Soc.* **1991**, *113*, 5282 and references therein. (b) Adams, R. D.; Wang, S. *Organometallics* **1985**, *4*, 1902. (c) Adams, R. D.; Wang, S. *J. Am. Chem. Soc.* **1987**, *109*, 924. (d) Martin, L. R.; Einstein, F. W. B.; Pomeroy, R. K. *Organometallics* **1988**, *7*, 294.

Scheme 1

$$Ru_3(CO)_{12} + 1.5K + 1.5Ph_2CO \xrightarrow[24\ hrs]{THF} {}^3/_4\ K_2[Ru_4(CO)_{13}]$$

$$K_2[Ru_4(CO)_{13}] \xrightarrow[2\ hrs]{2\ R_2PCl} Ru_4(CO)_{13}(\mu\text{-}PR_2)_2$$

Yields: 16% (R = OEt)
to 65% (R = N^{i}Pr$_2$)

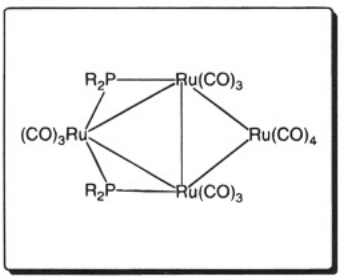

have found the 60-electron tetrahedral cluster $K_2[Ru_4(CO)_{13}]$[5] to be an excellent starting material for the synthesis of both phosphinidene- and phosphido-supported butterfly clusters by reaction with the appropriate dichloro- or monochlorophosphine, respectively. The success of this strategy prompted us to investigate the series of clusters $[Ru_4(CO)_{13}(\mu\text{-}PR_2)_2]$, where the substituent R could be readily modified and its effect on the bonding pattern in this novel type of molecule investigated.

The general outline for the preparation of **1a**−**f**, shown in Scheme 1, represents a rational route into a series of phosphido-bridge-supported tetranuclear clusters. The development of the chemistry of such M_4 and higher nuclearity clusters has been limited by the absence of rational synthetic routes to these compounds, and indeed, many structurally or electronically interesting clusters have never been examined simply because they are not accessible in workable yields.

Spectroscopic Features of 1a−**f.** In solution all of the molecules **1a**−**f** exhibit a single ^{31}P NMR resonance, indicating that the two μ-PR_2 groups are chemically and magnetically equivalent. The ^{31}P chemical shifts for **1a**,**b**,**e**,**f** are at higher field than normally observed for phosphido bridges in electron-precise Ru_4 clusters and intermediate between the latter values and shifts for μ_2-PR_2 ligands bridging "open" metal−metal bonds.[8] These upfield shifts correlate with increased Ru−P−Ru angles and an elongation of the Ru−Ru bonds bridged by the phosphido groups. Analysis of the chemical shift tensor components in related phosphido-bridged complexes suggests that the upfield shift is dominated by δ_{33}.[9] The ^{31}P chemical shifts for **1c**,**d** are, however, at consistently lower field (**1c**, δ 302.3 ppm; **1d**, δ 235.5 ppm). The substantial deshielding of the ^{31}P nucleus in the case of $P(OEt)_2$ and $P[N(Pr^i_2)_2]$ may be a consequence of the higher electronegativity of the phosphorus substituents, but a full explanation must await an analysis of the chemical shift tensor components currently being undertaken via ^{31}P CP/MAS studies.

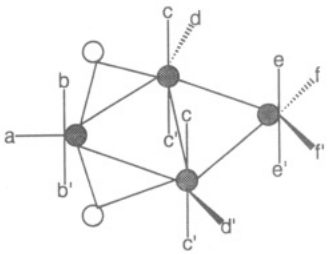

Figure 1. Carbonyl labeling scheme for the $Ru_4(CO)_{13}(\mu\text{-}PR_2)_2$ clusters.

In solution the ^{13}CO NMR spectra of **1a**−**f** consist of only five separate resonances with intensity ratios of 4:4:2:1:2 moving from low to high field. We attribute these signals to the sets of carbonyls designated cc′ (4), ee′ff′ (4), dd′ (2), a (1), and bb′ (2) as illustrated in Figure 1. These spectra presumably reflect the presence in solution of a plane of symmetry bisecting Ru(2) and Ru(4) (Ru(2) and Ru(3) in **1a**,**d**) and the midpoint of the Ru(1) and Ru(3) bond (Ru(1)−Ru(1a) bond in **1a**,**d**). In fact in **1a**,**d** the "hinge" $Ru(CO)_3$ groups are rendered equivalent by a crystallographic 2-fold axis and mirror plane, respectively. The assignment also implies that the four carbonyls designated ee′ff′ are in fast exchange under ambient conditions. For **1d** the unique ^{13}CO—^{31}P coupling ($^2J_{CP}$ = 10.6 Hz) to the carbonyls bb′ reflects the approximate *cis* relationship to the two phosphido bridges. None of the other sets of carbonyl ligands are coupled to the phosphorus atoms, although the signal assigned to cc′ is slightly broadened, perhaps indicating an unresolved, small coupling. These assignments are consistent with previous findings[10] on phosphido-bridged systems, where the trend observed is that $^2J_{PC}$ coupling constants are maximized at angles approaching 180° and minimized at 90° with a sign inversion (i.e. a near-zero value) at 107°. The angles associated with OC−Ru−P in **1d** for sites "a" (100.9(1)°), bb′ (89.1(1)° average), cc′ (94.5(1)° average), and "d" (99.6(1)°) lend support to these observations also. The assignments were confirmed by examining the low-temperature spectrum. At 198 K the exchange process for ee′ and ff′ had slowed and the peak ascribed to these four carbonyl ligands (δ 201.8 ppm) disappeared into the base line. The dynamic process could not, however, be frozen out. The remaining carbonyl resonances were unchanged at the lower temperature.

X-ray Structures of 1a−**d.** Crystals of **1a**,**d** crystallize with a half-molecule in the asymmetric unit of space groups $P2_12_12$ and $P2_1/m$, respectively. Thus, each molecule of **1a** has a crystallographic 2-fold axis and is rigidly planar. Molecules of **1d** possess mirror symmetry. The two remaining molecules crystallize in space group $P\bar{1}$. There are no unusual intermolecular contacts between molecules. Perspective views of the structures of **1a**−**d** are drawn in Figures 2−5. Important bond lengths and angles are summarized in Tables 2, 4, 6, and 8. Fractional atomic coordinates are tabulated in Tables 3, 5, 7, and 9. The molecular structures of **1a**−**d** all consist of a flattened-butterfly arrangement of ruthenium atoms with nearly coplanar

(8) Carty, A. J.; MacLaughlin, S. A.; Nucciarone, D. In *Phosphorus-31 NMR Spectroscopy in Stereochemical Analysis: Organic Compounds and Metal Complexes*; Verkade, J. G., Quinn, L. D., Eds.; VCH: New York, 1987; Chapter 16.

(9) Carty, A. J.; Fyfe, C. A.; Lettinga, M.; Johnson, S.; Randall, L. H. *Inorg. Chem.* **1989**, *28*, 4120.

(10) Randall, L. H.; Cherkas, A. A.; Carty, A. J. *Organometallics* **1989**, *8*, 568.

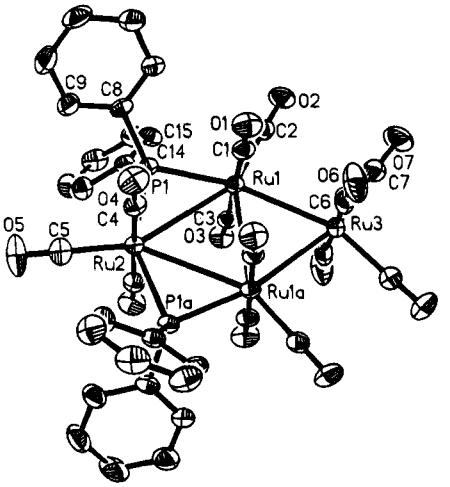

Figure 2. Molecular structure of $Ru_4(CO)_{13}(\mu\text{-}PPh_2)_2$ (**1a**).

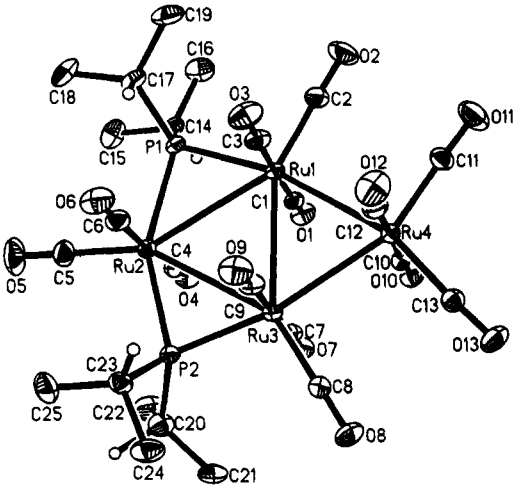

Figure 3. Molecular structure of $Ru_4(CO)_{13}(\mu\text{-}PPr^i_2)_2$ (**1b**).

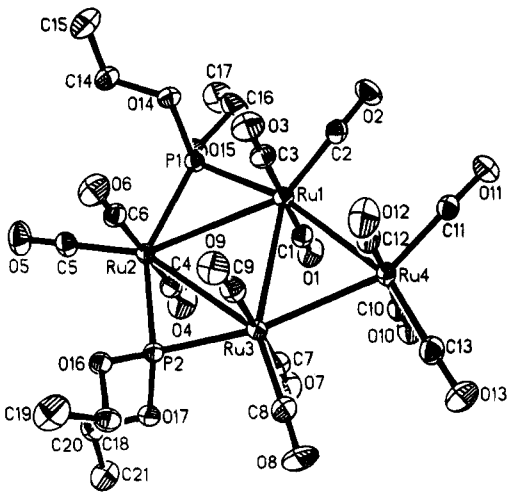

Figure 4. Molecular structure of $Ru_4(CO)_{13}[\mu\text{-}P(OEt)_2]_2$ (**1c**).

phosphido bridges. The dihedral angles between the planes defined by the two Ru_3 triangles in these related clusters span a small range of values, from 173° (R = NPr^i_2) to 180° (R = Ph), the near or total planarity of these systems resulting in an almost rhomboidal arrangement of ruthenium atoms. The two phosphido bridges in all cases adopt the same positions with respect to the metal framework, bridging adjacent ruthenium–ruthenium vectors. Indeed, the clusters

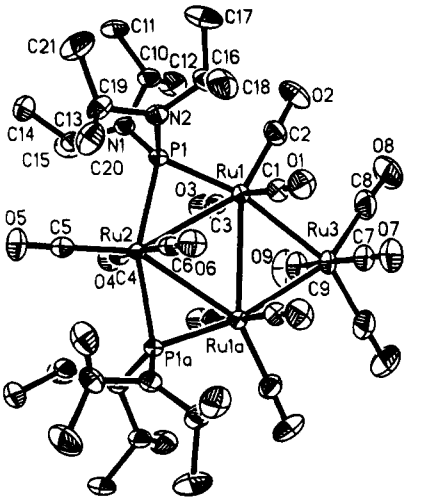

Figure 5. Molecular structure of $Ru_4(CO)_{13}[\mu\text{-}P(NPr^i_2)_2]_2$ (**1d**).

Table 2. Important Bond Lengths (Å) and Angles (deg) for 1a

Lengths			
Ru(1)–Ru(2)	3.1776(4)	Ru(1)–Ru(3)	2.9704(4)
Ru(1)–P(1)	2.3176(10)	Ru(1)–C(1)	1.933(3)
Ru(1)–C(2)	1.865(4)	Ru(1)–C(3)	1.940(3)
Ru(1)–Ru(1A)[a]	3.0509(4)	Ru(2)–P(1)	2.3605(9)
Ru(2)–C(4)	1.956(4)	Ru(2)–C(5)	1.884(6)
Ru(3)–C(6)	1.928(5)	Ru(3)–C(7)	1.917(4)
P(1)–C(8)	1.831(4)	P(1)–C(14)	1.831(4)

Angles			
Ru(2)–Ru(1)–Ru(3)	119.66(1)	Ru(2)–Ru(1)–P(1)	47.79(1)
Ru(3)–Ru(1)–P(1)	167.41(2)	Ru(2)–Ru(1)–Ru(1A)	61.31(1)
Ru(3)–Ru(1)–Ru(1A)	58.35(1)	P(1)–Ru(1)–Ru(1A)	109.09(2)
Ru(1)–Ru(2)–P(1)	46.65(2)	Ru(1)–Ru(2)–Ru(1A)	57.38(1)
P(1)–Ru(2)–Ru(1A)	104.02(2)	P(1)–Ru(2)–P(1A)	150.67(3)
Ru(1)–Ru(3)–Ru(1A)	63.29(1)	Ru(1)–P(1)–Ru(2)	85.56(1)
C(8)–P(1)–C(14)	103.1(2)		

[a] A indicates the symmetry transformation $-x, -y, z$.

can be viewed as consisting of an inner Ru_3 triangular arrangement of ruthenium atoms bridged by two phosphido ligands and an $Ru(CO)_4$ unit.

While the stereochemistry at Ru(4) (labeled Ru(3) for **1a**,**d**) is approximately octahedral with two axial carbonyls, two equatorial carbonyls, and two Ru–Ru bonds, the coordination environment of the three remaining ruthenium atoms is irregular. The two hinge atoms Ru(1) and Ru(3) (Ru(1) and Ru(1a)) have bonds to three CO groups, three other metal atoms, and a phosphido bridge. The stereochemistry is best described as distorted pentagonal bipyramidal. For the Ru(2) wingtip atom there are three Ru–CO bonds, two Ru–Ru interactions, and two Ru–P bonds. The overall coordination geometry is again that of a distorted pentagonal bipyramid. The most important structural detail to be noted, however, is the presence of elongated metal–metal and metal–phosphorus vectors. For comparison purposes compilations of Ru–Ru distances for a wide range of tetranuclear clusters suggest that a "normal" Ru–Ru bond length can be considered to be within the range 2.70–2.95 Å.[4a] The Ru–Ru distance in $Ru_3(CO)_{12}$ (2.85 Å average)[11] lies somewhere in the middle of this range of values. Any Ru–Ru contact

(11) Churchill, M. R.; Hollander, F. J.; Hutchinson, J. P. *Inorg. Chem.* **1977**, *16*, 2655.

Table 3. Atomic Coordinates (×10⁴) and Isotropic Displacement Coefficients (Å² × 10³) for $Ru_4(CO)_{13}(\mu\text{-}PPh_2)_2\cdot 2CHCl_3$ (1a)

	x	y	z	U(eq)[a]
Ru(1)	691.4(2)	824.0(2)	−156.6(2)	22.50(6)
Ru(2)	0	0	1976.0(3)	21.5(1)
Ru(3)	0	0	−2050.2(3)	26.4(1)
P(1)	1007.6(7)	1245.4(6)	1518.8(8)	23.0(2)
O(1)	2959(2)	−216(2)	−230(3)	44(1)
O(2)	1834(3)	2194(2)	−1395(3)	45(1)
O(3)	−1577(2)	1852(1)	−39(3)	39(1)
O(4)	2377(3)	−904(2)	2008(3)	44(1)
O(5)	0	0	4282(3)	67(2)
60(1)	2110(3)	−1200(2)	−2080(3)	60(1)
O(7)	1330(3)	1081(2)	−3575(3)	63(1)
C(1)	2090(3)	144(2)	−222(3)	30(1)
C(2)	1409(3)	1672(2)	−922(3)	31(1)
C(3)	−763(3)	1450(2)	−106(3)	28(1)
C(4)	1505(3)	−584(2)	1972(3)	29(1)
C(5)	0	0	3417(4)	38(2)
C(6)	1320(4)	−755(3)	−2001(3)	41(1)
C(7)	837(4)	709(3)	−2986(3)	38(1)
C(8)	2510(3)	1322(2)	1985(3)	28(1)
C(9)	2727(4)	1278(3)	3028(4)	43(1)
C(10)	3850(4)	1285(4)	3402(4)	55(2)
C(11)	4782(4)	1345(4)	2737(4)	55(2)
C(12)	4576(4)	1390(3)	1700(4)	47(2)
C(13)	3447(3)	1392(2)	1336(3)	35(1)
C(14)	368(3)	2256(2)	1906(3)	24(1)
C(15)	501(3)	2968(2)	1283(3)	34(1)
C(16)	−23(4)	3731(3)	1543(3)	42(1)
C(17)	−665(4)	3801(3)	2428(4)	43(1)
C(18)	−804(4)	3110(3)	3055(4)	43(1)
C(19)	−283(3)	2338(2)	2796(3)	34(1)
C(1S)	2072(4)	3456(3)	−5621(4)	48(2)
Cl(1S)	1471(1)	2675(1)	−4830(1)	60(1)
Cl(2S)	3580(1)	3478(1)	−5464(1)	79(1)
Cl(3S)	1452(2)	4433(1)	−5369(2)	108(1)

[a] Equivalent isotropic U, defined as one-third of the trace of the orthogonalized U_{ij} tensor.

Table 4. Important Bond Lengths (Å) and Angles (deg) for 1b

Lengths			
Ru(1)−Ru(2)	3.1993(3)	Ru(1)−Ru(3)	3.0762(3)
Ru(1)−Ru(4)	2.9138(3)	Ru(1)−P(1)	2.3245(7)
Ru(2)−Ru(3)	3.1597(3)	Ru(2)−P(1)	2.3820(7)
Ru(2)−P(2)	2.3835(7)	Ru(3)−Ru(4)	2.9229(3)
Ru(3)−P(2)	2.3267(8)	P(1)−C(14)	1.864(3)
P(1)−C(17)	1.863(3)	P(2)−C(20)	1.877(3)
P(2)−C(23)	1.871(4)		

Angles			
Ru(2)−Ru(1)−Ru(3)	60.42(1)	Ru(2)−Ru(1)−Ru(4)	118.76(1)
Ru(3)−Ru(1)−Ru(4)	58.34(1)	Ru(2)−Ru(1)−P(1)	47.93(2)
Ru(3)−Ru(1)−P(1)	108.34(2)	Ru(4)−Ru(1)−P(1)	166.65(2)
Ru(1)−Ru(2)−Ru(3)	57.86(1)	Ru(1)−Ru(2)−P(1)	46.43(2)
Ru(3)−Ru(2)−P(1)	104.27(2)	Ru(1)−Ru(2)−P(2)	104.96(2)
Ru(3)−Ru(2)−P(2)	47.11(2)	P(1)−Ru(2)−P(2)	151.29(3)
Ru(1)−Ru(3)−Ru(2)	61.72(1)	Ru(1)−Ru(3)−Ru(4)	58.05(1)
Ru(2)−Ru(3)−Ru(4)	119.77(1)	Ru(1)−Ru(3)−P(2)	110.34(2)
Ru(2)−Ru(3)−P(2)	48.64(2)	Ru(4)−Ru(3)−P(2)	168.36(2)
Ru(1)−Ru(4)−Ru(3)	63.61(1)	Ru(1)−P(1)−Ru(2)	85.64(2)
Ru(2)−P(2)−Ru(3)	84.25(2)	C(14)−P(1)−C(17)	109.0(1)
C(20)−P(2)−C(23)	101.3(2)		

above 3.0 Å is unusually long. Ruthenium−ruthenium distances longer than 3.40 Å have been interpreted as nonbonding.[12] Although the bond elongation effect is noticeable in each of compounds **1a−d**, with the averages of the five Ru−Ru distances being similar in all cases, there is a marked difference as to the distribution of the elongation patterns. Indeed, varying the organic

(12) Carty, A. J.; MacLaughlin, S. A.; Taylor, N. J. *J. Organomet. Chem.* **1981**, *204*, C27.

Table 5. Atomic Coordinates (×10⁴) and Isotropic Displacement Coefficients (Å² × 10³) for $Ru_4(CO)_{13}(\mu\text{-}PPr^i_2)_2\cdot CHCl_3$ (1b)

	x	y	z	U(eq)[a]
Ru(1)	1298.6(2)	787.5(2)	1946.0(2)	25.78(8)
Ru(2)	3673.9(2)	1229.3(2)	2799.5(2)	27.79(9)
Ru(3)	1867.5(2)	3132.6(2)	2027.4(2)	24.40(8)
Ru(4)	−272.3(2)	2632.7(2)	1258.6(2)	28.47(9)
P(1)	2791.5(8)	−375.0(6)	2602.4(6)	27.5(3)
P(2)	3629.1(7)	3151.3(6)	2714.1(6)	27.4(2)
O(1)	2804(2)	811(2)	−89(2)	42(1)
O(2)	−217(3)	−818(2)	1379(2)	69(1)
O(3)	−285(3)	715(2)	3951(2)	55(1)
O(4)	5103(2)	1093(2)	754(2)	48(1)
O(5)	5951(3)	419(3)	3660(3)	87(2)
O(6)	2216(3)	1129(2)	4853(2)	62(1)
O(7)	3387(2)	3181(2)	0(2)	41(1)
0(8)	1126(2)	5512(2)	1637(2)	49(1)
O(9)	380(3)	3074(2)	4066(2)	53(1)
O(10)	1221(2)	2694(2)	−781(2)	46(1)
O(11)	−2051(3)	1223(2)	682(3)	76(1)
O(12)	−1850(3)	2671(3)	3253(2)	68(1)
O(13)	−1357(2)	4909(2)	662(2)	53(1)
C(1)	2242(3)	849(2)	658(2)	32(1)
C(2)	356(3)	−209(3)	1606(3)	41(1)
C(3)	298(3)	787(3)	3206(3)	39(1)
C(4)	4567(3)	1180(3)	1496(3)	35(1)
C(5)	5092(4)	726(3)	3330(3)	51(1)
C(6)	2736(3)	1192(3)	4089(3)	40(1)
C(7)	2798(3)	3127(3)	743(2)	31(1)
C(8)	1407(3)	4604(3)	1786(2)	32(1)
C(9)	900(3)	3064(3)	3300(3)	36(1)
C(10)	729(3)	2643(3)	−3(3)	36(1)
C(11)	−1373(3)	1732(3)	903(3)	45(1)
C(12)	−1196(3)	2632(3)	2547(3)	44(1)
C(13)	−926(3)	4077(3)	900(3)	37(1)
C(14)	3724(3)	−1265(3)	1753(2)	36(1)
C(15)	4960(4)	−1693(3)	2033(3)	58(2)
C(16)	3062(4)	−2158(3)	1503(3)	56(2)
C(17)	2238(3)	−1219(3)	3753(2)	37(1)
C(18)	3233(4)	−1797(3)	4289(3)	62(2)
C(19)	1303(4)	−1998(3)	3666(3)	58(2)
C(20)	4905(3)	3937(3)	2021(3)	44(1)
C(21)	4486(3)	4992(3)	1479(3)	48(1)
C(22)	5851(4)	3326(4)	1381(4)	73(2)
C(23)	3439(3)	3679(3)	3920(2)	36(1)
C(24)	3128(4)	4902(3)	3864(3)	54(2)
C(25)	4516(4)	3327(4)	4453(3)	59(2)
C(26S)	8342(4)	6329(3)	3006(3)	56(2)
Cl(1S)	7813(1)	7629(1)	3282(1)	81(1)
Cl(2S)	7120(2)	5602(1)	2909(1)	104(1)
Cl(3S)	9202(1)	5687(1)	3873(1)	97(1)

[a] Equivalent isotropic U, defined as one-third of the trace of the orthogonalized U_{ij} tensor.

substituent of the phosphido bridge exerts a significant influence on the bonding within the cluster framework, a fact confirmed by EHMO studies (*vide infra*).

A comparison of the core bond lengths associated with **1a−d** is given in Table 10. These values reveal that there is a similar pattern of three long and two normal metal−metal interactions in each cluster, the bond lengthening being primarily limited to the inner Ru_3 triangle spanned by the two phosphido bridges and the $Ru(CO)_4$ unit. We will comment on the electronic reasons for these changes later.

This pattern of a combination of long and normal bond lengths is not unique to this class of bis(phosphido) cluster. It has been noted previously that for tetranuclear frameworks where the valence electron count exceeds that predicted by the EAN rule, the effect of electronic supersaturation is a lengthening of two, three, or four of the metal−metal bonding distances. Thus, for example, the cluster $[Os_4(CO)_{12}(\mu_3\text{-}S)_2]$, which consists of a closed-butterfly array of osmium atoms, was

Table 6. Important Bond Lengths (Å) and Angles (deg) for 1c

Lengths			
Ru(1)—Ru(2)	3.2316(2)	Ru(1)—Ru(3)	3.0316(2)
Ru(1)—Ru(4)	2.9359(3)	Ru(1)—P(1)	2.2643(8)
Ru(2)—Ru(3)	3.2182(3)	Ru(2)—P(1)	2.3222(8)
Ru(2)—P(2)	2.3317(8)	Ru(3)—Ru(4)	2.9262(3)
Ru(3)—P(2)	2.2594(8)	P(1)—O(14)	1.609(2)
P(1)—O(15)	1.604(3)	P(2)—O(16)	1.616(3)
P(2)—O(17)	1.603(2)		

Angles			
Ru(2)—Ru(1)—Ru(3)	61.74(1)	Ru(2)—Ru(1)—Ru(4)	120.38(1)
Ru(3)—Ru(1)—Ru(4)	58.70(1)	Ru(2)—Ru(1)—P(1)	45.93(2)
Ru(3)—Ru(1)—P(1)	107.65(2)	Ru(4)—Ru(1)—P(1)	166.30(2)
Ru(1)—Ru(2)—Ru(3)	56.07(1)	Ru(1)—Ru(2)—P(1)	44.48(2)
Ru(3)—Ru(2)—P(1)	100.53(2)	Ru(1)—Ru(2)—P(2)	100.64(2)
Ru(3)—Ru(2)—P(2)	44.58(2)	P(1)—Ru(2)—P(2)	145.03(3)
Ru(1)—Ru(3)—Ru(2)	62.19(1)	Ru(1)—Ru(3)—Ru(4)	59.02(1)
Ru(2)—Ru(3)—Ru(4)	121.15(1)	Ru(1)—Ru(3)—P(2)	108.60(2)
Ru(2)—Ru(3)—P(2)	46.42(2)	Ru(4)—Ru(3)—P(2)	167.52(2)
Ru(1)—Ru(4)—Ru(3)	62.28(1)	Ru(1)—P(1)—Ru(2)	89.59(2)
Ru(2)—P(2)—Ru(3)	88.99(2)	O(14)—P(1)—O(15)	104.2(1)
O(16)—P(2)—O(17)	104.7(1)		

found to possess two elongated (3.047(1) Å average) and three normal (2.930(1) Å average) Os—Os bonding distances, the former value representing the nonadjacent metal—metal bonds spanning the wingtip and hinge metal atom positions.[3i] The 64-electron flattened-butterfly cluster $[Ru_4(CO)_8(\mu\text{-}H)_2\{CH_3{=}C(H)C(H){=}NPr^i_2\}_2]$ was found to possess three long and two normal (2.8203(8) Å average) Ru—Ru interactions, the hinge (3.1409(6) Å) and two nonadjacent wingtip to hinge (3.1237(8) Å average) metal—metal distances exhibiting the elongation, presumably due to an only partially delocalized molecular orbital antibonding with respect to the metal core.[3h] Finally, the molecular structure of the rigidly planar molecule $[Ru_4(CO)_{10}(\mu\text{-}PPh_2)_4]$ revealed a lengthening of the four peripheral ruthenium—ruthenium distances (3.050(1) Å average), while the hinge vector remained unaffected (2.8355(7) Å).[3j] There are also recent examples of M_3 and M_5 cluster systems displaying expanded metal frameworks.[3]

EHMO Calculations. All calculations were performed using the CACAO program.[13] Following up on the earlier work of Proserpio and Mealli[14] we have carried out EHMO calculations on the models $[Ru_4(CO)_{13}(\mu\text{-}PH_2)_2]$, $[Ru_4(CO)_{13}\{\mu\text{-}P(CH_3)_2\}_2]$, $[Ru_4(CO)_{13}\{\mu\text{-}P(NH_2)_2\}_2]$, and $[Ru_4(CO)_{13}\{\mu\text{-}P(OH)_2\}_2]$ in order to attempt to correlate their electronic and structural relationships, specifically the effect of changing the alkyl/alkoxy/amino substituents on the bridging phosphido groups. Before describing the analysis, it is pertinent to comment further on the transition-metal fragments composing **1a**—**f**. The molecule $[Ru_4(CO)_{13}(\mu\text{-}PR_2)_2]$ is constructed from a triangular, electron-precise $Ru_3(CO)_9(\mu\text{-}PR_2)_2$ fragment by adding a bridging $Ru(CO)_4$ unit. The latter $Ru(CO)_4$ fragment is isolobal with CH_2, and it is the addition of an extra two-electron donor to $Ru_3(CO)_9(\mu\text{-}PR_2)_2$ which provides the additional electron pair beyond the 48-electron closed shell. A representation of the overall energy level diagram for these molecules with the fragment MO's for $Ru_3(CO)_9(\mu\text{-}PH_2)_2$ on the left, for $Ru(CO)_4$ on the right, and for the molecule as a whole (with idealized C_{2v} symmetry) in the middle is shown in Figure 6. The orbital contributions to the HOMO, the SHOMO, and the third highest occupied MO are illustrated in Figure 7. The detailed picture shows a $2b_2$ HOMO which is antibonding with respect to the Ru—Ru interactions in the $Ru_3(\mu\text{-}PR_2)_2$ triangle. There is also a small component of Ru—P σ bonding in this MO. The two next highest occupied MO's are strongly Ru—Ru bonding within the two Ru_3 triangles. A third strongly bonding b_2 MO lies at the same energy as the t_{2g} manifold. These calculations also illustrate that there is only a small energy difference between the $2b_2$ and $3a_1$ orbitals (~0.4 eV for R = H). The relative ordering of these two molecular orbitals is thus very sensitive to the overall molecular structure. Indeed, using the X-ray crystallographic data as structural parameters for these calculations demonstrated that the HOMO is actually bonding in nature for R = Me, OH ($3a_1$) and it is the occupied SHOMO ($2b_2$) which is responsible for cluster expansion. It is worth noting, however, that when this situation arises

(13) Mealli, C.; Proserpio, D. M. *J. Chem. Educ.* **1990**, *67*, 399.
(14) Mealli, C.; Proserpio, D. M. *J. Am. Chem. Soc.* **1990**, *112*, 5484.

Table 7. Atomic Coordinates ($\times 10^4$) and Isotropic Displacement Coefficients ($Å^2 \times 10^3$) for $Ru_4(CO)_{13}[\mu\text{-}P(OEt)_2]_2 \cdot {}^1/_2C_6H_6$ (1c)

	x	y	z	U(eq)[a]
Ru(1)	2203.9(3)	2409.0(2)	3665.4(1)	23.33(8)
Ru(2)	3160.2(3)	4356.1(2)	2169.0(1)	22.82(8)
Ru(3)	3762.7(3)	1421.9(2)	2207.8(1)	25.26(9)
Ru(4)	2957.2(3)	−251.0(2)	3625.7(2)	25.78(9)
P(1)	1925.9(9)	4490.4(7)	3408.3(5)	24.5(3)
P(2)	4223(1)	3029.9(7)	1281.5(5)	25.4(3)
O(1)	5200(3)	2276(2)	4260(2)	45(1)
O(2)	800(3)	2027(3)	5327(2)	46(1)
O(3)	−850(3)	2657(3)	3099(2)	44(1)
O(4)	6149(3)	4250(3)	2783(2)	57(1)
O(5)	3257(4)	6982(2)	1414(2)	56(1)
O(6)	142(3)	4669(3)	1555(2)	48(1)
O(7)	6855(3)	1199(3)	2720(2)	53(1)
O(8)	4952(4)	−663(3)	1312(2)	66(1)
O(9)	731(3)	1741(3)	1619(2)	46(1)
O(10)	5981(3)	−470(2)	4212(2)	45(1)
O(11)	1570(3)	−916(2)	5302(2)	42(1)
O(12)	5(3)	−203(3)	3001(2)	54(1)
O(13)	4258(4)	−2665(3)	3022(2)	59(1)
O(14)	217(3)	5204(2)	3460(1)	32(1)
O(15)	2699(3)	5145(2)	3920(1)	32(1)
O(16)	3361(3)	3349(2)	504(1)	30(1)
O(17)	5951(3)	2860(2)	961(1)	33(1)
C(1)	4130(4)	2269(3)	4021(2)	30(1)
C(2)	1331(4)	2169(3)	4693(2)	30(1)
C(3)	294(4)	2516(3)	3291(2)	32(1)
C(4)	5057(4)	4243(3)	2563(2)	35(1)
C(5)	3226(4)	5998(3)	1694(2)	33(1)
C(6)	1253(4)	4525(3)	1779(2)	32(1)
C(7)	5689(4)	1274(3)	2572(2)	35(1)
C(8)	4510(5)	114(3)	1655(2)	40(1)
C(9)	1812(4)	1601(3)	1874(2)	32(1)
C(10)	4863(4)	−314(3)	3976(2)	33(1)
C(11)	2083(4)	−646(3)	4678(2)	31(1)
C(12)	1087(4)	−139(3)	3219(2)	37(1)
C(13)	3765(4)	−1760(3)	3226(2)	38(1)
C(14)	−133(4)	6513(3)	3137(2)	42(1)
C(15)	−1769(5)	6888(4)	3080(3)	68(2)
C(16)	2285(5)	5024(4)	4769(2)	50(2)
C(17)	2877(6)	5908(4)	5091(3)	60(2)
C(18)	3556(4)	2457(3)	−26(2)	37(1)
C(19)	2486(5)	2931(4)	−613(3)	57(2)
C(20)	6518(4)	3900(3)	504(2)	41(1)
C(21)	8175(4)	3565(4)	400(3)	52(2)
C(1S)	−1494(9)	410(8)	23(10)	124(5)
C(2S)	−874(15)	−10(8)	690(7)	115(5)
C(3S)	627(18)	−437(6)	665(7)	128(6)

[a] Equivalent isotropic U, defined as one-third of the trace of the orthogonalized U_{ij} tensor.

Table 8. Important Bond Lengths (Å) and Angles (deg) for 1d

Lengths			
Ru(1)—Ru(2)	3.1064(3)	Ru(1)—Ru(3)	2.9721(3)
Ru(1)—P(1)	2.3482(7)	Ru(1)—C(1)	1.951(4)
Ru(1)—C(2)	1.855(3)	Ru(1)—C(3)	1.935(4)
Ru(1)—Ru(1A)[a]	3.1589(3)	Ru(2)—P(1)	2.3959(7)
Ru(2)—C(4)	1.944(5)	Ru(2)—C(5)	1.891(4)
Ru(2)—C(6)	1.951(5)	Ru(3)—C(7)	1.941(6)
P(1)—N(1)	1.706(3)	P(1)—N(2)	1.703(3)
N(1)—C(10)	1.489(4)	N(1)—C(13)	1.485(4)
N(2)—C(16)	1.478(4)	N(2)—C(19)	1.497(3)
Angles			
Ru(2)—Ru(1)—Ru(3)	117.06(1)	Ru(2)—Ru(1)—P(1)	49.76(1)
Ru(3)—Ru(1)—P(1)	166.50(1)	Ru(2)—Ru(1)—Ru(1A)	59.44(1)
Ru(3)—Ru(1)—Ru(1A)	57.90(1)	P(1)—Ru(1)—Ru(1A)	109.17(1)
Ru(1)—Ru(2)—P(1)	48.44(1)	Ru(1)—Ru(2)—Ru(1A)	61.12(1)
P(1)—Ru(2)—Ru(1A)	109.52(2)	P(1)—Ru(2)—P(1A)	157.65(2)
Ru(1)—Ru(3)—Ru(1A)	64.20(1)	Ru(1)—P(1)—Ru(2)	81.80(1)
N(1)—P(1)—N(2)	107.7(1)		

[a] A indicates the symmetry transformation x, $^1/_4 - y$, z.

Table 9. Atomic Coordinates ($\times 10^4$) and Isotropic Displacement Coefficients ($Å^2 \times 10^3$) for $Ru_4(CO)_{13}[\mu\text{-}P(NPr^i_2)_2]_2$ (1d)

	x	y	z	U(eq)[a]
Ru(1)	555.4(3)	3160.5(1)	396.3(2)	23.23(7)
Ru(2)	2363.1(3)	2500	2786.2(3)	18.4(1)
Ru(3)	−1359.4(4)	2500	−1736.6(3)	33.0(1)
P(1)	2115.4(8)	3482.9(3)	2348.4(7)	20.3(2)
N(1)	1405(3)	3869(1)	3333(2)	25(1)
N(2)	3589(2)	3822(1)	2233(2)	26(1)
O(1)	2713(3)	3136(1)	−1163(2)	46(1)
O(2)	−455(3)	4266(1)	−842(3)	65(1)
O(3)	−1908(2)	3140(1)	1585(2)	44(1)
O(4)	−196(3)	2500	3860(3)	34(1)
O(5)	4501(4)	2500	5445(3)	51(1)
O(6)	4501(3)	2500	1213(3)	37(1)
O(7)	835(4)	2500	−3256(3)	54(1)
O(8)	−2766(3)	3534(1)	−3214(3)	81(1)
O(9)	−3841(4)	2500	−580(4)	75(2)
C(1)	1930(3)	3121(1)	−581(3)	34(1)
C(2)	−81(4)	3840(2)	−386(3)	39(1)
C(3)	−999(3)	3129(1)	1144(3)	32(1)
C(4)	745(5)	2500	3464(4)	25(1)
C(5)	3695(5)	2500	4449(4)	29(2)
C(6)	3737(5)	2500	1804(4)	27(1)
C(7)	85(6)	2500	−2629(4)	41(2)
C(8)	−2210(4)	3152(2)	−2661(3)	53(1)
C(9)	−2837(7)	2500	−903(5)	53(2)
C(10)	835(3)	4425(1)	2807(3)	31(1)
C(11)	1471(4)	4921(1)	3662(3)	44(1)
C(12)	−776(4)	4477(2)	2393(4)	47(1)
C(13)	1536(3)	3713(1)	4695(3)	31(1)
C(14)	2711(4)	4005(2)	5766(3)	47(1)
C(15)	145(4)	3755(2)	5028(4)	46(1)
C(16)	3650(4)	4143(1)	1080(3)	38(1)
C(17)	3542(4)	4789(2)	1180(4)	57(2)
C(18)	4900(4)	3995(2)	589(3)	48(1)
C(19)	4798(3)	3825(1)	3451(3)	34(1)
C(20)	6026(3)	3445(2)	3440(3)	44(1)
C(21)	5380(4)	4400(2)	3935(4)	57(2)

[a] Equivalent isotropic U, defined as one-third of the trace of the orthogonalized U_{ij} tensor.

the energy levels of the HOMO and SHOMO are nearly degenerate ($\Delta = 0.03$ eV).

The net consequences of this EHMO picture are that the 32nd pair of cluster valence electrons in these 64-electron butterfly clusters occupies an orbital antibonding with respect to one Ru_3 triangle, accounting nicely for the pattern of cluster expansion. Within the frontier orbital region of these clusters three electron pairs provide delocalized metal−metal bonding, with the $2b_2$ orbital being only weakly bonding with respect to the "outer" $Ru_3(CO)_{10}$ fragment. The overlap populations for **1a**−**d** (Table 11) roughly confirm that Ru—P bonding is strongest in **1c** and, conversely, Ru—Ru bonding in the $Ru(\mu\text{-}PR_2)Ru(\mu\text{-}PR_2)Ru$ unit is weakest.

Table 10. Core Bond Lengths

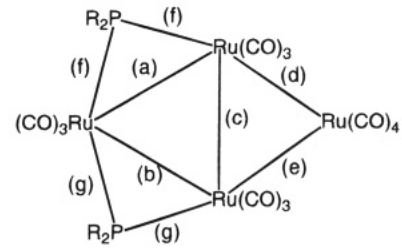

bond type	R = Ph	R = ^{i}Pr	R = OEt	R = N^{i}Pr$_2$
Ru—Ru (a)	3.1776(4)	3.1597(3)	3.2318(2)	3.1064(3)
Ru—Ru(b)	3.1776(4)	3.1993(3)	3.2182(3)	3.1064(3)
Ru—Ru (c)	3.0509(4)	3.0762(3)	3.0316(2)	3.1589(3)
Ru—Ru (d)	2.9074(4)	2.9229(3)	2.9359(3)	2.9721(3)
Ru—Ru(e)	2.9074(4)	2.9138(3)	2.9262(3)	2.9721(3)
Ru—P (f) av	2.339(1)	2.353(1)	2.293(1)	2.372(1)
Ru—P (g) av	2.339(1)	2.355(1)	2.296(1)	2.372(1)

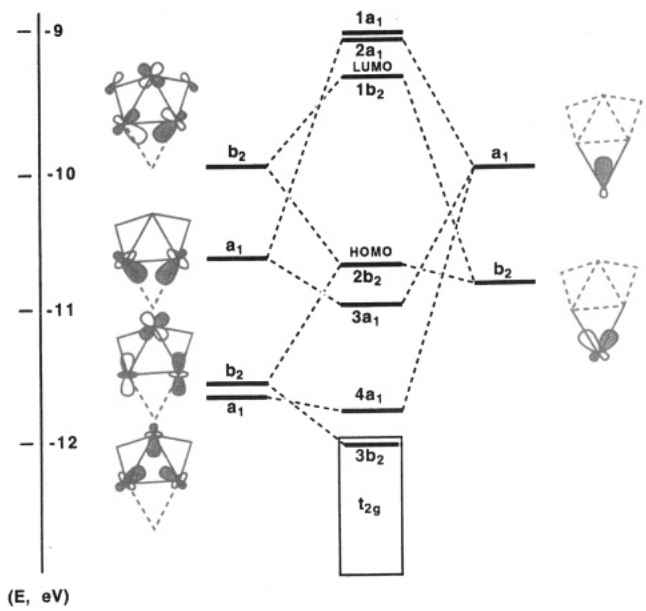

Figure 6. Qualitative representation of the frontier molecular orbitals for the model cluster $Ru_4(CO)_{13}(\mu\text{-}Ph_2)_2$ with idealized C_{2v} symmetry.

Closer examination of the bonding distances in Table 10, however, for the π-electron-donating (NPr^i_2) and the more electronegative (OEt) substituents on the phosphido bridge reveals that there is an apparent change in the way in which this electron richness is alleviated. The bond lengths associated with **1d** (R = NPr^i_2) indicate that the bonding pattern is approaching one where there are five "long" (2.9724(4)−3.1582(4) Å) metal−metal interactions and four long Ru—P bonding distances (2.372(1) Å average). Conversely, the bonding arrangement found for **1c** (R = OEt) indicates two very long Ru—Ru bonds (3.2323(4) and 3.2183(4) Å), one long bond (3.0323(4) Å), and two normal (2.9362(4) and 2.9256(4) Å) interactions where the two longest distances are associated with the phosphido-bridged metal−metal vectors and the two shortest represent those formed by the lone $Ru(CO)_4$ unit. The Ru—P distances are also noticeably shorter (2.295(1) Å average). There

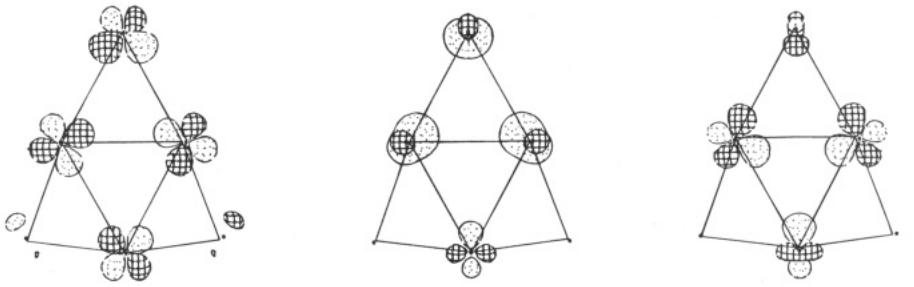

Figure 7. Projections of the ruthenium- and phosphorus-based orbitals contributing to the HOMO, SHOMO, and THOMO in the model cluster $Ru_4(CO)_{13}(\mu\text{-}PH_2)_2$.

Table 11. EHMO Overlap Populations for Cluster 1[a]

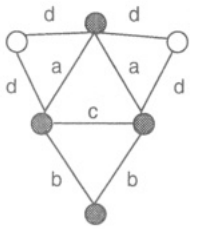

	R in μ-PR_2			
	H	CH_3	NH_2	OH
a	0.078	0.056	0.066	0.046
b	0.189	0.200	0.191	0.192
c	0.155	0.136	0.121	0.146
d	0.476	0.506	0.518	0.547

[a] Calculations performed using X-ray bond lengths where available.

thus appears to be an interdependence within the Ru-(μ-PR_2)Ru(μ-PR_2)Ru chain between the Ru—P and Ru—Ru bond lengths and the organic substituent on phosphorus. Our EHMO analyses of these isolated fragments indicate that the presence of the high-lying lone pairs on the nitrogen atoms leads to a destabilizing effect of the P—N molecular orbitals. The resultant effect leads to a weakening of the P—Ru interactions due to a reduced overlap between the molecular orbitals of the metal framework and the phosphido bridges. The lone pairs on oxygen for the OEt substituent lie much lower in energy and thus have no destabilizing effect on the O—P or Ru—P bonds.

We are currently investigating the chemical/electrochemical oxidation and reduction properties of these fascinating molecules in order to further cement the electronic/structural relationships.

Acknowledgment. We are grateful to the Natural Sciences and Engineering Research Council of Canada for financial support of this work in the form of operating and equipment grants (to A.J.C.) and a scholarship (to J.F.C.). G.H. thanks the SERC for a Postdoctoral Fellowship. We also thank Prof. C. Mealli for providing a copy of the CACAO program.

Supplementary Material Available: For **1a—d** structural analyses, complete crystallographic data (Tables S1, S6, S11, and S16), anisotropic displacement coefficients (Tables S2, S7, S12, and S17), complete bond lengths (Tables S3, S8, S13, and S18) and angles (Tables S4, S9, S14, and S19), and hydrogen atom coordinates (Tables S5, S10, S15, and S20) (29 pages). Ordering information is given on any current masthead page. Structure factors (Tables S21—S24, 91 pages) are available from the authors upon request.

OM940188T